14th International Conference on Structural Safety and Reliability - ICOSSAR'25
1-6 June, 2025 - Los Angeles California, USA
R. Ghanem, E. Johnson, S. Masri and A. Olivier (Eds)

# BAYESIAN NONLINEAR FINITE ELEMENT MODEL UPDATING OF A FULL-SCALE BRIDGE COLUMN: INSIGHTS FROM CALIBRATION OF INHERENT DAMPING MODEL

**ENRIQUE G. SIMBORT ZEBALLOS[1], MUKESH K. RAMANCHA[1], RODRIGO ASTROZA[2] AND JOEL P. CONTE[1]**

[1]University of California, San Diego
Department of Structural Engineering
9500 Gilman Drive, La Jolla, CA 92093, USA
egsimbortzeballos@ucsd.edu, mramanch@ucsd.edu, jpconte@ucsd.edu

[2]Universidad de los Andes
Faculty of Engineering and Applied Sciences
Mons. Alvaro del Portillo 12455 Las Condes, Santiago, Chile
rastroza@miuandes.cl

**Key words:** Bayesian Inference, Digital Twin, Inherent Damping, Model Updating, Structural Health Monitoring, Full-Scale Structural Systems, Earthquake.

**Abstract.** This study presents a Bayesian framework for calibrating a nonlinear finite element (FE) model of a full-scale reinforced concrete (RC) bridge column tested on the Large High-Performance Outdoor Shake Table (LHPOST) at University of California, San Diego (UCSD). Using experimental input-output data from three selected earthquake ground motions (GMs) of increasing intensity, material, damping, and noise parameters are calibrated via the Transitional Markov Chain Monte Carlo (TMCMC) method. The calibrated FE model yields improved predictive accuracy, with postprocessed effective modal damping ratios extracted from the calibrated FE model exhibiting strong response amplitude dependence both within and across seismic excitations.

## 1 INTRODUCTION

Digital twin-based approaches for structural health monitoring (SHM) and damage prognosis (DP) are emerging as powerful framework for intelligent infrastructure management by integrating physics-based FE models with measurement data. Bayesian updating of nonlinear FE models using input-output measurement data allows iterative calibration that accounts for noise, parameter uncertainty, and model form error, supporting probabilistic assessment and improved predictive reliability over a structure's lifespan [1].

Nonlinear FE models have advanced significantly, capturing key seismic response features, including stiffness degradation, concrete cracking, plastic hinging, and collapse mechanisms under strong ground motions (GM) [2]. However, predictive accuracy hinges on properly calibrating uncertain parameters such as material properties, boundary conditions, and damping. Bayesian calibration is increasingly adopted for its ability to incorporate prior knowledge, manage measurement noise, and quantify posterior uncertainty [3].

Among various modeling uncertainties, inherent damping—representing energy dissipation mechanisms not explicitly modeled through material nonlinearity—remains particularly

challenging to quantify and calibrate [4–7]. These mechanisms include internal friction, strain-rate effects, hysteresis in non-structural components, interface friction, and energy radiation into the soil. Rayleigh damping is commonly used as a practical approximation, introducing viscous forces proportional to mass and stiffness matrices [4]. Despite its simplicity, it poses challenges in nonlinear analyses, particularly in selecting and calibrating the damping coefficients, for which no consensus exists [5].

Recent experimental studies have shown that inherent damping is response amplitude-dependent [4,8]. Damping ratios identified from low-amplitude vibrations (e.g., ambient tests) often underestimate dissipation under seismic loads, especially in nonlinear systems where damage and stiffness degradation modify dissipation mechanisms. Despite its significance, this amplitude dependency is rarely incorporated into Bayesian model updating workflows.

This paper addresses this gap by presenting a Bayesian nonlinear FE model updating framework for calibrating material and Rayleigh damping parameters. Using the calibrated Rayleigh coefficients, the amplitude-dependent behavior of inherent damping is examined. The study leverages data from a full-scale RC bridge column, designed per modern seismic codes and tested on the NEES@UCSD LHPOST under a sequence of ten recorded earthquake GMs of systematically increasing intensity. From this dataset, three excitations (EQ1–EQ3) are selected to investigate the evolution of damping parameters with increasing response amplitude.

A distributed plasticity FE model is developed and updated using the TMCMC method [9], including Rayleigh damping parameters. The results elucidate the interplay between damping behavior and nonlinear structural response, provide insights into the identifiability of damping parameters across varying excitation amplitudes, and inform the development of physics-based digital twins for seismic response analysis.

The remainder of the paper details the experimental program (Section 2), nonlinear FE modeling and inherent damping formulation (Section 3), Bayesian inference via TMCMC (Section 4), model calibration and results (Section 5), and conclusions (Section 6).

## 2 EXPERIMENTAL PROGRAM AND CALIBRATION DATA

A full-scale RC bridge column was tested in 2010 on the LHPOST at UCSD. The experimental program aimed to assess seismic performance of RC bridge columns under strong GMs. The column had a circular cross-section (1.22 m diameter) and a height of 7.32 m, designed for a target displacement ductility of four under EQ3, corresponding to the Safety Evaluation Earthquake (SEE) (5% probability of exceedance in 50 years), promoting flexural-dominated nonlinear response.

The specimen included 1.55% longitudinal and 0.95% volumetric confining reinforcement. The as-built static axial load at the base, under gravity loading, was 2.53 MN (5.3% axial load ratio). Further construction and material details are in [10].

The specimen was instrumented with 278 sensors—including strain gauges, potentiometers, accelerometers, and GPS devices—to capture both global and local response measures. To simulate superstructure inertia, a 2.32 MN concrete block was cast atop the column. The test sequence involved ten recorded ground motions of increasing intensity applied along the shake table's longitudinal (E-W) direction.

This study uses data from the first three excitations (EQ1–EQ3) to capture the gradual transition from quasi-linear elastic to nonlinear behavior. EQ1 induced with minor cracking;

EQ2 initiated localized yielding; and EQ3 reached the target ductility with spalling and distributed cracking. This progression enables study of response amplitude-dependent damping behavior and calibration of material and damping parameters across distinct nonlinear regimes.

For the Bayesian calibration, time histories of absolute horizontal acceleration, rotational acceleration, and relative horizontal displacement at the superstructure's center of mass are used—capturing essential translational and rotational dynamics.

## 3 FE MODEL OF FULL-SCALE RC BRIDGE COLUMN SPECIMEN

### 3.1 Nonlinear FE Model

The nonlinear FE model of the 7.32 m long RC bridge column is developed using the OpenSees analysis framework [2], employing two nonlinear force-based fiber-section Euler-Bernoulli beam-column elements [11] to represent the column. The bottom and top elements are assigned two and five Gauss-Lobatto integration points, respectively, along their lengths (Figure 1b). The tributary length of the first integration point is initialized based on an empirical estimate of the plastic hinge length ( $L_{ph}$ ) [12], which serves as the prior expected value in the Bayesian updating process.

Each element cross-section is fiber-discretized, with uniaxial constitutive models used for material response (Figure 1c, d). Concrete04 captures the behavior of confined and unconfined concrete [13], while SteelDRC is used for longitudinal reinforcement [14]. Material properties are derived from experimental tests [10] or empirical models, with confined concrete properties adjusted to account for transverse confinement effects.

The corotational formulation is employed to account for geometric nonlinear effects. The footing is assumed fixed, and the bridge superstructure is idealized by applying a lumped mass ( $M=236.6\,kN{\cdot}s^2/m$ ) and rotational mass moment of inertia ( $M_{rot}=1.04\cdot10^4\,kN{\cdot}m^2/g$ ) applied at the column top node.

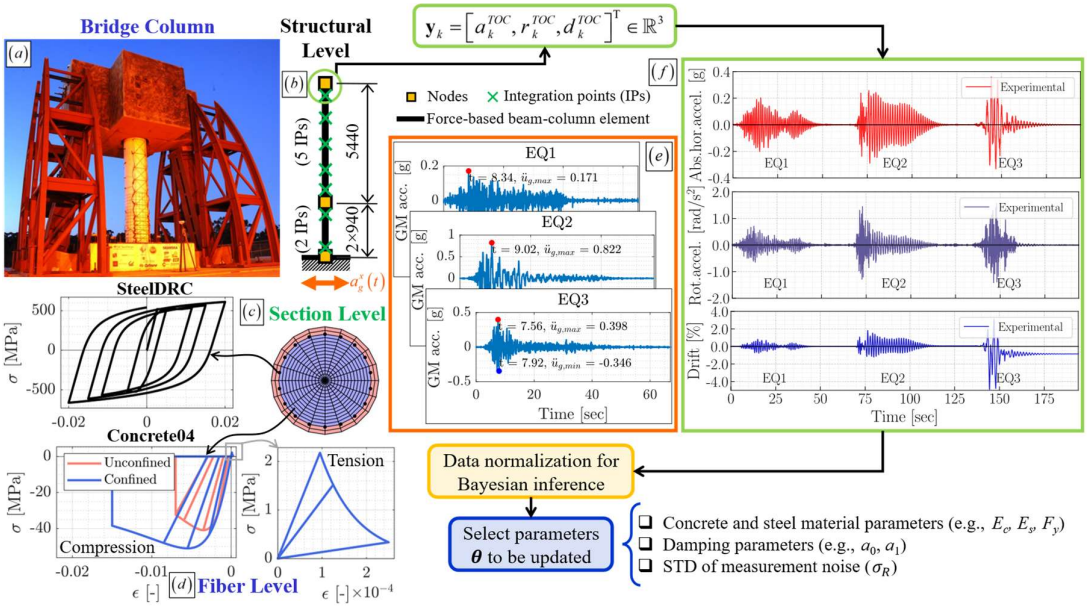


**Figure 1:** FE model hierarchy of bridge column. Input GMs and experimental response measurements

### 3.2 Inherent Damping Modeling

In this study, inherent damping, representing energy dissipation mechanisms beyond the hysteretic energy dissipated through inelastic material behavior, is modeled using the Rayleigh damping model, which is proportional to the mass matrix $\mathbf{M}$ and initial stiffness matrix $\mathbf{K}_0$. The damping matrix $\mathbf{C}^i$ corresponding to earthquake excitation $i$ (EQ$i$) is defined as:

$$\mathbf{C}^i = a^i_{0,0}\mathbf{M} + a^i_{1,0}\mathbf{K}_0 \tag{1}$$

where $a^i_{0,0}$ and $a^i_{1,0}$ are the mass- and stiffness-proportional damping coefficients to be calibrated. The Rayleigh damping model structure is retained throughout the Bayesian model updating process; specifically, the form of $\mathbf{C}^i$ remains fixed, while the damping coefficients $a^i_{0,0}$ and $a^i_{1,0}$ are updated based on experimental measurements for each EQ$i$.

The use of the initial stiffness matrix $\mathbf{K}_0$ aligns with established nonlinear dynamic analysis practice, providing a stable and consistent formulation for calibrating damping and material parameters. Although $\mathbf{K}_0$-based damping may overestimate energy dissipation post-yielding, it preserves proportional damping assumptions and avoids spurious energy injection and numerical instability commonly associated with tangent stiffness-based models [5,15]. When used with distributed plasticity beam-column elements, the sensitivity of structural response to the damping formulation is significantly reduced, making classical Rayleigh damping with $\mathbf{K}_0$ a robust and widely accepted choice. This provides a suitable starting point for investigating amplitude-dependent inherent damping, while maintaining compatibility with standard nonlinear analysis practices. More advanced formulations may be explored in future work to refine dissipation modeling under progressive nonlinear damage.

Following model Bayesian calibration, the evolution of effective modal damping is analyzed to evaluate the amplitude-dependent behavior of inherent damping during seismic response. At each time interval $t_w$ of the structural response to an earthquake input ($kt_w, k = 1, 2, \ldots$), the tangent stiffness matrix $\mathbf{K}^i_{T,kt_w}$ is extracted from the nonlinear analysis, and the following "instantaneous" eigenvalue analysis is performed:

$$\left[\mathbf{K}^i_{T,\,kt_w} - \left(\omega^i_{n,\,kt_w}\right)^2 \mathbf{M}\right]\boldsymbol{\phi}^i_{n,\,kt_w} = \mathbf{0} \tag{2}$$

to obtain the instantaneous mode shapes $\boldsymbol{\phi}^i_{n,\,kt_w}$ and circular frequencies $\omega^i_{n,\,kt_w}$ corresponding to the time instants $kt_w$. Using the calibrated Rayleigh damping matrix $\mathbf{C}^i$ and the instantaneous modal properties, the instantaneous modal damping coefficient for mode $n$ is defined as

$$c^i_{n,\,kt_w} = \left(\boldsymbol{\phi}^i_{n,\,kt_w}\right)^T \mathbf{C}^i \boldsymbol{\phi}^i_{n,\,kt_w} \tag{3}$$

and the corresponding instantaneous effective damping ratio at time $kt_w$ is calculated as

$$\xi^{i,*}_{n,\,kt_w} = \frac{1}{2}\frac{c^i_{n,\,kt_w}}{\omega^i_{n,\,kt_w} m^i_{n,\,kt_w}} \tag{4}$$

where $m^i_{n,\,kt_w} = \left(\boldsymbol{\phi}^i_{n,\,kt_w}\right)^T \mathbf{M}\boldsymbol{\phi}^i_{n,\,kt_w}$ is the instantaneous generalized modal mass.

By tracking $\xi_{n,kt_w}^{i,*}$ over time and across earthquakes of varying intensity, the amplitude-dependent evolution of inherent damping is quantified. As will be shown in Section 5.3, although the Rayleigh damping matrix ($\mathbf{C}^i$) remains fixed during a given earthquake, the effective modal damping ratios exhibit significant time- and amplitude-dependent variability during the structural response to that earthquake.

## 4 BAYESIAN NONLINEAR FE MODEL UPDATING AND TRANSITIONAL MARKOV CHAIN MONTE CARLO METHOD

### 4.1 Bayesian Nonlinear FE Model Updating

Consider a structural system at discrete time step $k$, with measured input and output vectors $\mathbf{u}_k \in \mathbb{R}^{n_\mathbf{u}}$ and $\mathbf{y}_k \in \mathbb{R}^{n_\mathbf{y}}$, where $n_\mathbf{u}$ and $n_\mathbf{y}$ are the number of input and output measurement channels. Given measurements over $N$ time steps, the input-output histories are: $\mathbf{u}_{1:N} = \left[\mathbf{u}_1^T, \mathbf{u}_2^T, ..., \mathbf{u}_N^T\right]^T \in \mathbb{R}^{(n_\mathbf{u} \times N)\times 1}$ and $\mathbf{y}_{1:N} = \left[\mathbf{y}_1^T, \mathbf{y}_2^T, ..., \mathbf{y}_N^T\right]^T \in \mathbb{R}^{(n_\mathbf{y} \times N)\times 1}$.

The input-output measurement dataset is denoted $\mathcal{D} = \left\{\left(\mathbf{u}_1, \mathbf{y}_1\right), ..., \left(\mathbf{u}_N, \mathbf{y}_N\right)\right\} \equiv \left(\mathbf{u}_{1:N}, \mathbf{y}_{1:N}\right)$.

Let $\mathbf{y}_k^{FE} = \mathbf{h}_k\left(\mathbf{u}_{1:k}; \boldsymbol{\theta}\right) \in \mathbb{R}^{n_\mathbf{y}}$ represent the output response of the FE model $\mathbf{h}\left(\boldsymbol{\theta}\right)$ at time step $k$ when subjected to the measured input time history $\mathbf{u}_{1:k} \in \mathbb{R}^{(n_\mathbf{u} \times k)\times 1}$. The FE model $\mathbf{h}\left(\boldsymbol{\theta}\right)$ is parameterized by the unknown parameter vector $\boldsymbol{\theta} = \left[\theta_1, \theta_2, ..., \theta_{n_\boldsymbol{\theta}}\right]^T \in \mathbb{R}^{n_\boldsymbol{\theta}}$, where $n_\boldsymbol{\theta}$ denotes the number of unknown parameters. The vector $\boldsymbol{\theta}$ may include any unknown, time-invariant parameters characterizing the FE model. Differences between measured $\mathbf{y}$ and FE-predicted $\mathbf{y}^{FE}$ responses arise from input/output measurement noise, model parameter uncertainty, and model form uncertainty which is not considered in this study.

Three key components are required to perform Bayesian model updating: (1) measurement data $\mathcal{D}$, (2) a prior PDF of the unknown parameters $p\left(\boldsymbol{\theta}\right)$, and (3) a measurement equation (joint physical-statistical model). The measurement equation is defined at time step $k$ as:

$$\mathbf{y}_k = \mathbf{h}_k\left(\mathbf{u}_{1:k}; \boldsymbol{\theta}\right) + \mathbf{w}_k; \quad k \in \left[1, 2, ..., N\right] \tag{5}$$

where $\mathbf{w}_k = \left[w_{1,k}, ..., w_{n_\mathbf{y},k}\right]^T \in \mathbb{R}^{n_\mathbf{y}}$ is the additive measurement noise, modeled as zero-mean Gaussian with i.i.d. components, statistically independent across channels and time. Each $w_{i,k}$ denotes the discrepancy between measured and FE predicted output at the $i^{th}$ output measurement channel at time step $k$. Under these assumptions, the likelihood function for the full dataset $\mathcal{D}$ is expressed as:

$$p\left(\mathbf{y} \mid \mathbf{u}, \boldsymbol{\theta}, \boldsymbol{\sigma}\right) = \prod_{k=1}^{N} p\left(\mathbf{y}_k \mid \mathbf{u}_{1:k}, \boldsymbol{\theta}, \boldsymbol{\sigma}\right) = \prod_{k=1}^{N} \frac{1}{\left(2\pi\right)^{n_\mathbf{y}/2}} \left|\boldsymbol{\Sigma}\right|^{-1/2} \exp\left\{-\frac{1}{2}\left[\mathbf{y}_k - \mathbf{h}_k\left(\mathbf{u}_{1:k}; \boldsymbol{\theta}\right)\right] \boldsymbol{\Sigma}^{-1} \left[\mathbf{y}_k - \mathbf{h}_k\left(\mathbf{u}_{1:k}; \boldsymbol{\theta}\right)\right]^T\right\} \tag{6}$$

where $\boldsymbol{\Sigma}$ is a diagonal covariance matrix associated with the measurement noise, and $\boldsymbol{\sigma}$ denotes the standard deviations of measurement noise across the output channels.

Bayesian model updating aims to determine the posterior PDF of the unknown parameters

$\boldsymbol{\theta}$ given the measurement dataset $\mathcal{D}$. By Bayes' theorem, the posterior PDF is given by:

$$p(\boldsymbol{\theta},\boldsymbol{\sigma}\,|\,\mathcal{D}) \equiv p(\boldsymbol{\theta},\boldsymbol{\sigma}\,|\,\mathbf{u},\mathbf{y}) = \frac{p(\mathbf{y}\,|\,\mathbf{u},\boldsymbol{\theta},\boldsymbol{\sigma}) \times p(\boldsymbol{\theta},\boldsymbol{\sigma})}{p(\mathbf{u},\mathbf{y})} \tag{7}$$

where $p(\boldsymbol{\theta},\boldsymbol{\sigma})$ is the prior PDF, incorporating our prior belief about the unknown FE model parameters, and $p(\mathbf{u},\mathbf{y})$ represents the evidence, serving as a normalizing constant.

### 4.2 Transitional Markov Chain Monte Carlo (TMCMC) Method

The TMCMC method is a simulation-based Bayesian inference framework that samples from the joint posterior distribution of the unknown parameter vector $\boldsymbol{\theta}$, referred to as target PDF hereafter. TMCMC does not assume Gaussian priors or posteriors. Instead of sampling directly from the target PDF, TMCMC constructs a sequence of intermediate distributions that progressively transition from the prior to the posterior, expressed as

$$p(\boldsymbol{\theta}\,|\,\mathbf{u}_{1:N},\mathbf{y}_{1:N})_j \propto p(\mathbf{y}_{1:N}\,|\,\mathbf{u}_{1:N},\boldsymbol{\theta})^{\beta_j} \times p(\boldsymbol{\theta}) \tag{8}$$

where index $j$ denotes the stage number, and $\beta_j$ is the tempering parameter controlling the influence of the likelihood function at stage $j$. At the initial stage $(j=0)$, $p(\boldsymbol{\theta}\,|\,\mathbf{u}_{1:N},\mathbf{y}_{1:N})_0 = p(\boldsymbol{\theta})$ with $\beta_0 = 0$. The process evolves progressively, eventually converging to the target posterior distribution at the final stage $(j=m)$, where $\beta_m = 1$ and $p(\boldsymbol{\theta}\,|\,\mathbf{u}_{1:N},\mathbf{y}_{1:N})_m$ coincides with the target posterior PDF $p(\boldsymbol{\theta}\,|\,\mathbf{u}_{1:N},\mathbf{y}_{1:N})$. At each stage *j*, TMCMC approximates the intermediate PDF $p(\boldsymbol{\theta}\,|\,\mathbf{u}_{1:N},\mathbf{y}_{1:N})_j$ by weighting, resampling, and perturbing the particles drawn from the previous stage. Resampling is performed via random sampling, and particle perturbation is conducted using the MCMC Metropolis-Hastings algorithm. For further details, see [3,9].

## 5 BAYESIAN FE MODEL UPDATING OF FULL-SCALE RC BRIDGE COLUMN

### 5.1 Prior Distributions

To capture the RC column's response evolution from elastic (EQ1) to moderately nonlinear (EQ3) behavior, a set of structural and damping parameters is selected for Bayesian calibration. The vector of unknown parameter, $\boldsymbol{\theta}$, includes material properties governing flexural behavior, Rayleigh damping coefficients per excitation, and measurement noise standard deviations. For concrete, updated parameters include Young's modulus ($E_c$), tensile strength ($f_{ct}$), peak compressive strain ($\varepsilon_{cu}$) and strength ($f'_{cu}$), and a tensile softening parameter ($\beta$). For steel, the updated parameters are Young's modulus ($E_s$), yield strength ($F_y$), and yield plateau length ($\varepsilon_{sh}$). The plastic hinge length ($L_{ph}$)—a geometric parameter—governs the spread of inelastic deformations.

The Rayleigh damping coefficients $a^i_{0,0}$ and $a^i_{1,0}$, where $i = 1,2,3$, correspond to EQ1–EQ3, and enable explicit modeling of inherent damping effects across varying amplitude levels.

Measurement noise standard deviations ($\sigma_a$, $\sigma_r$, and $\sigma_d$) are also treated as unknowns to account for noise in the acceleration, rotational acceleration, and displacement response measurements, respectively, and to indirectly capture model form uncertainties.

The selection of these updating parameters was informed by a preliminary global sensitivity analysis (GSA) based on Sobol sensitivity indices. In total, 18 parameters are updated: 9 material and structural parameters, 6 damping coefficients, and 3 noise terms. Thus,

$$\boldsymbol{\theta} = \left[ E_c, f_{ct}, f'_{cu}, \varepsilon_{c0u}, \beta, E_s, F_y, \varepsilon_{sh}, L_{ph}, a^1_{0,0}, \ldots, a^3_{1,0}, \sigma_a, \sigma_r, \sigma_d \right]^T \in \mathbb{R}^{18}.$$

Prior distributions for the updated parameters are defined using engineering judgment and experimental data, including concrete and steel tests and system identification from white noise excitation. The experimentally determined (PEER) parameters [10] serve as reference values for constructing these priors. All distributions are assumed mutually independent for simplicity. Table 1 summarizes the updated model parameters, along with their corresponding reference values and prior specifications, expressed in the physical domain. For parameters assigned uniform priors, only the support bounds are indicated, as these fully define the distributions.

**Table 1:** Prior distributions of FE model parameters

| **Prior Distribution of Material and Geometric Parameters** | | | | | | | | | |
|---|---|---|---|---|---|---|---|---|---|
| $\theta$ | $E_c$ | $f'_{cu}$ | $\varepsilon_{c0u}$ | $f_{ct}$ | $\beta$ | $E_s$ | $F_y$ | $\varepsilon_{sh}$ | $L_{ph}$ |
| $\theta^{ref}$ | $2.29\times10^4$ [MPa] | –40.9 [MPa] | –0.0035 [–] | 2.11 [MPa] | 0.1 [–] | $1.96\times10^5$ [MPa] | 519.0 [MPa] | 0.011 [–] | 0.94 [m] |
| Type | $\mathcal{N}_{[l_{E_c}, u_{E_c}]}$ | $\mathcal{N}_{[l_{f'_{cu}}, u_{f'_{cu}}]}$ | $\mathcal{N}_{[l_{\varepsilon_{c0u}}, u_{\varepsilon_{c0u}}]}$ | $\mathcal{U}_{[l_{f_{ct}}, u_{f_{ct}}]}$ | $\mathcal{U}_{[l_\beta, u_\beta]}$ | $\mathcal{N}_{[l_{E_s}, u_{E_s}]}$ | $\mathcal{N}_{[l_{F_y}, u_{F_y}]}$ | $\mathcal{U}_{[l_{\varepsilon_{sh}}, u_{\varepsilon_{sh}}]}$ | $\mathcal{N}_{[l_{L_{ph}}, u_{L_{ph}}]}$ |
| $\mu_\theta^{prior}$ | $1.0E_c^{ref}$ | $1.0f_{cu}^{\prime\ ref}$ | $1.0\varepsilon_{c0u}^{ref}$ | – | – | $1.0E_s^{ref}$ | $1.0F_y^{ref}$ | – | $1.0L_{ph}^{ref}$ |
| $\sigma_\theta^{prior}$ | $0.3\mu_{E_c}^{prior}$ | $0.2\mu_{f'_{cu}}^{prior}$ | $0.2\mu_{\varepsilon_{c0u}}^{prior}$ | – | – | $0.2\mu_{E_s}^{prior}$ | $0.2\mu_{F_y}^{prior}$ | – | $0.4\mu_{L_{ph}}^{prior}$ |
| $\frac{[l_\theta, u_\theta]}{\mu_\theta^{prior}}$ | [0.8,1.2] | [0.85,1.15] | [0.86,1.15] | – | – | [0.92,1.08] | [0.98,1.10] | – | [0.65,1.95] |
| $\frac{[l_\theta, u_\theta]}{\theta^{ref}}$ | – | – | – | [1.7,4.0] | [0.5,7.0] | – | – | [0.36,1.1] | – |
| **Prior Distribution of Damping and Noise Parameters** | | | | | | | | | |
| $\theta$ | $a^1_{0,0}$ | $a^1_{1,0}$ | $a^2_{0,0}$ | $a^2_{1,0}$ | $a^3_{0,0}$ | $a^3_{1,0}$ | $\sigma_a$ | $\sigma_r$ | $\sigma_d$ |
| $\theta^{ref}$ | 0.6006 [$s^{-1}$] | $2.64\times10^{-4}$ [s] | 0.5349 [$s^{-1}$] | $3.66\times10^{-4}$ [s] | 0.3518 [$s^{-1}$] | $5.86\times10^{-4}$ [s] | 0.2 [g] | 0.7 [rad·$s^{-2}$] | 0.06 [m] |
| Type | $\mathcal{U}_{[l_{a^1_0}, u_{a^1_0}]}$ | $\mathcal{U}_{[l_{a^1_1}, u_{a^1_1}]}$ | $\mathcal{U}_{[l_{a^2_0}, u_{a^2_0}]}$ | $\mathcal{U}_{[l_{a^2_1}, u_{a^2_1}]}$ | $\mathcal{U}_{[l_{a^3_0}, u_{a^3_0}]}$ | $\mathcal{U}_{[l_{a^3_1}, u_{a^3_1}]}$ | Half-$\mathcal{N}$ | Half-$\mathcal{N}$ | Half-$\mathcal{N}$ |
| $\mu_\theta^{prior}$ | – | – | – | – | – | – | 0.0 | 0.0 | 0.0 |
| $\sigma_\theta^{prior}$ | – | – | – | – | – | – | $0.2\sigma_a^{ref}$ | $0.2\sigma_r^{ref}$ | $0.2\sigma_d^{ref}$ |
| $\frac{[l_\theta, u_\theta]}{\theta^{ref}}$ | [0.0,0.72] | [0.0,6.1] | [0.1,0.77] | [0.0,4.4] | [0.1,0.96] | [0.0,3.1] | – | – | – |

FE model updating of the RC column is performed using the TMCMC method (Section 4.2) and input-output measurement data from EQ1 to EQ3. At each TMCMC stage, $N_p = 2000$ particles approximate the intermediate joint PDF, with 5 MCMC steps per perturbation step.

For the considered load case, TMCMC run completes in ~ 75.5 minutes on Frontera HPC (TACC) using 40 Cascade Lake (CLX) nodes (56 cores per node, 192GB RAM).

All parameter estimates are normalized with respect to their corresponding reference values for comparative analysis (e.g. $\tilde{\theta}_i = \theta_i / \theta_i^{ref}$, where $\theta_i^{ref}$ is the reference value (see Table 1).

## 5.2 Discussion of Results

**Posterior Distributions of Calibrated Parameters.** Table 2 presents the TMCMC-calibrated posterior distributions of normalized material, damping, and noise parameters, including sample mean ($\bar{\mu}_{\tilde{\theta}}^{post}$) and coefficients-of-variation ($\delta_{\tilde{\theta}}^{post}$). The posterior distributions of the material parameters show pronounced peaks, with $\delta_{\tilde{\theta}}^{post}$ typically in the $10^{-3}$ to $10^{-4}$ range. The small dispersion in the normalized posterior of the parameters such as $\tilde{E}_c$, $\tilde{E}_s$, $\tilde{F}_y$ and $\tilde{L}_{ph}$ indicates high statistical confidence in their calibrated values and reflect the sensitivity of the FE model response to these parameters under increasing seismic excitation intensity.

**Table 2:** Sample mean and coefficient of variation of normalized posterior TMCMC samples

| | **Material and Geometric Parameters** | | | | | | | | |
|---|---|---|---|---|---|---|---|---|---|
| $\tilde{\theta}$ | $\tilde{E}_c$ | $\tilde{f}'_{cu}$ | $\tilde{\varepsilon}_{c0u}$ | $\tilde{f}_{ct}$ | $\tilde{\beta}$ | $\tilde{E}_s$ | $\tilde{F}_y$ | $\tilde{\varepsilon}_{sh}$ | $\tilde{L}_{ph}$ |
| $\bar{\mu}_{\tilde{\theta}}^{post}$ | 0.92 | 0.85 | 1.11 | 3.01 | 2.69 | 0.92 | 1.03 | 0.85 | 1.80 |
| $\delta_{\tilde{\theta}}^{post}$ | $7.06\times10^{-4}$ | $1.68\times10^{-3}$ | $4.27\times10^{-3}$ | $4.05\times10^{-3}$ | $6.34\times10^{-2}$ | $5.36\times10^{-4}$ | $3.98\times10^{-4}$ | $9.79\times10^{-3}$ | $7.52\times10^{-4}$ |
| | **Damping and Noise Parameters** | | | | | | | | |
| $\tilde{\theta}$ | $\tilde{a}^1_{0,0}$ | $\tilde{a}^1_{1,0}$ | $\tilde{a}^2_{0,0}$ | $\tilde{a}^2_{1,0}$ | $\tilde{a}^3_{0,0}$ | $\tilde{a}^3_{1,0}$ | $\tilde{\sigma}_a$ | $\tilde{\sigma}_r$ | $\tilde{\sigma}_d$ |
| $\bar{\mu}_{\tilde{\theta}}^{post}$ | 0.1656 | 6.073 | 0.1017 | 1.926 | 0.1032 | 2.125 | 0.1096 | 0.1417 | 0.1251 |
| $\delta_{\tilde{\theta}}^{post}$ | $5.30\times10^{-3}$ | $3.18\times10^{-3}$ | $1.13\times10^{-2}$ | $8.69\times10^{-3}$ | $2.13\times10^{-2}$ | $9.69\times10^{-3}$ | $9.39\times10^{-3}$ | $8.80\times10^{-3}$ | $4.39\times10^{-3}$ |

Figure 2 presents box plots illustrating the stage-wise evolution of normalized posterior samples for key material parameters obtained from the TMCMC algorithm. The red horizontal lines indicate the normalized reference values from the PEER report, and the green dashed lines mark the bounds of the normalized prior distributions (fixed at all TMCMC stages; see Eq. (8)).

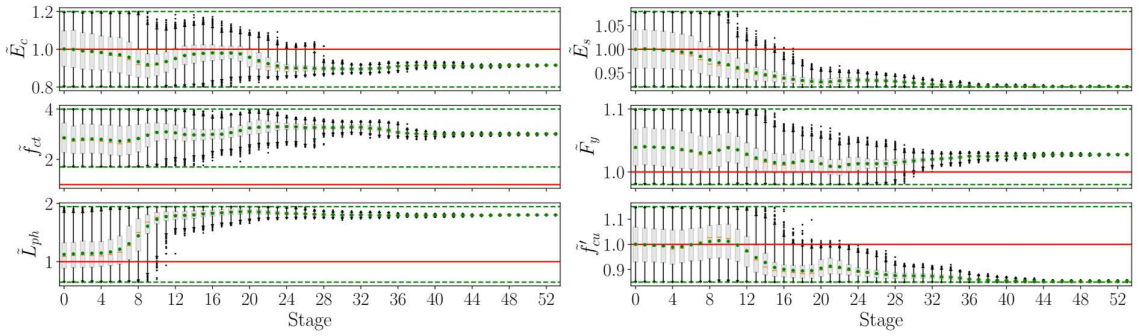


**Figure 2:** Stage-wise Evolution of Normalized Posterior Distributions for Material Parameters

In the early TMCMC stages (1–10), the posterior samples exhibit high variability, reflecting significant epistemic uncertainty. Between stages 10–24, the distributions' spread narrows considerably, with box plots contracting—indicating growing confidence in the inferred

parameters. In the final stages (24–53), the posterior distributions become sharply concentrated, revealing well-converged estimates with low residual uncertainty.

The posterior distributions of the normalized Rayleigh damping coefficients are visualized using the pair plot in Figure 3. The diagonal subplots show kernel density estimates and histograms of the marginal posteriors, with corresponding $\delta_{\tilde{\theta}}^{post}$ values in the order of $10^{-3}$, indicating narrow and well-constrained posterior distributions.

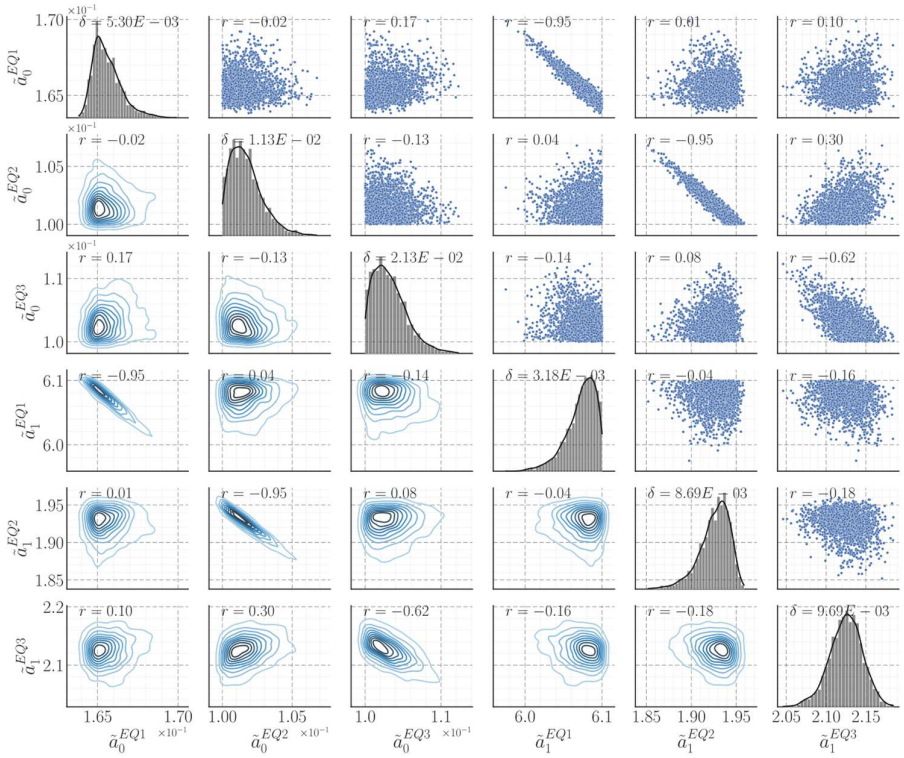


**Figure 3:** Pair plot of posterior samples for updated damping parameters obtained via TMCMC

A strong negative correlation (e.g., $r = -0.95$) is observed between the normalized mass- and stiffness-proportional damping coefficients across excitations. This is consistent with Rayleigh damping formulation, where for a given modal frequency $\omega_n$, an increase in $a_{0,0}^i$ is offset by a decrease in $a_{1,0}^i$ to achieve the target damping ratio $\xi_n^i$ for the $n$th mode (Eq.(1)). However, the strength of this trade-off diminishes as the structural response departs from quasi-linear behavior (Figure 3). As mild-to-moderate material nonlinearity develops, additional energy dissipation mechanisms—hysteretic effects—progressively dominate the response.

The posterior means of the standard deviations of the noise channels show $\delta_{\tilde{\theta}}$ below $10^{-2}$, indicating stable inference and confirming the appropriateness of the Gaussian error model.

These results confirm that the TMCMC-based Bayesian updating yields highly concentrated posterior distributions with physically interpretable correlations, reinforcing the robustness of the inferred parameter set for nonlinear FE modeling of RC column under seismic excitation.

**Model Validation and Predictive Capability.** The accuracy of the calibrated model is

assessed by comparing its simulated structural response against experimental measurements, both for the earthquakes used in calibration (EQ1-EQ3) and for an independent (subsequent) prediction case (EQ4) of comparable intensity. Figure 4 and Figure 5 illustrate the time histories of absolute horizontal acceleration and drift, respectively, along with the evolution of the first two effective modal damping ratios (Eq. (4)) throughout the sequence of seismic excitations.

Substantial improvements in response prediction are observed following Bayesian updating: the acceleration relative root mean square errors (RRMSE) drops from 96%, 95%, and 68% (prior model) to 47%, 29%, and 26% (updated model) for EQ1–EQ3, respectively. Likewise, the drift RRMSE improves from 89%, 93%, and 51% to 41%, 29%, and 10%, respectively. These RRMSE reductions reflect improved fidelity in capturing the column's nonlinear dynamic behavior, confirming the effectiveness of the inferred parameter set.

The predictive capability of the model is further examined using EQ4 (not included in the calibration process). The updated model produces RRMSE values of 53% for acceleration and 20% for drift–significantly lower than the prior model's 101% and 52%, respectively–demonstrating generalizability of the calibrated parameter set under similar excitation intensity.

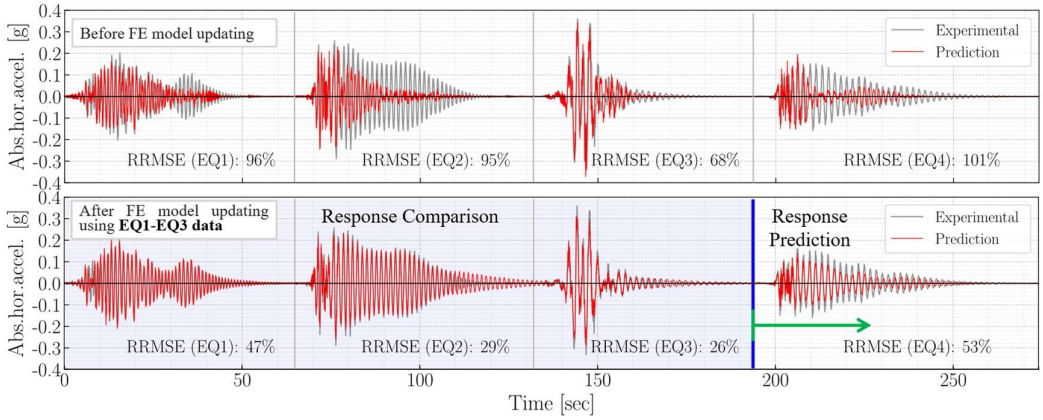


**Figure 4: A**bsolute horizontal acceleration response comparison before and after calibration

The evolution of the instantaneous effective modal damping ratios (Eq. (4)) is derived from the nonlinear FE response predicted using the posterior sample means all calibrated parameters (see Table 2), following the methodology outlined in Section 3.2.

Figure 5 reveals a clear amplitude dependency of the instantaneous effective inherent modal damping ratios, both within individual seismic excitation and across excitations of increasing intensity. For EQ1 through EQ4, the effective modal damping ratios exhibit pronounced temporal evolution, strongly correlated with the time-varying drift response amplitudes. This trend is particularly evident in the second mode, where the damping ratio $\xi^{i,*}_{2,kt_w}$, closely follows the envelope of the drift response. The close alignment between the time-dependent instantaneous effective modal damping ratios and the structural response amplitude provides indirect evidence of the dependence of inherent damping on structural response amplitude.

The elevated modal damping ratios under EQ1 deviate from expected trends, exceeding those of EQ2 and EQ3 despite its lower intensity. This likely stems from model limitations, as the FE formulation may not capture dominant low-amplitude dissipation mechanisms—micro-cracking, bond-slip, or friction—causing the inferred damping to compensate for these unmodeled hysteretic effects, thus overestimating damping estimates in the quasi-linear regime.

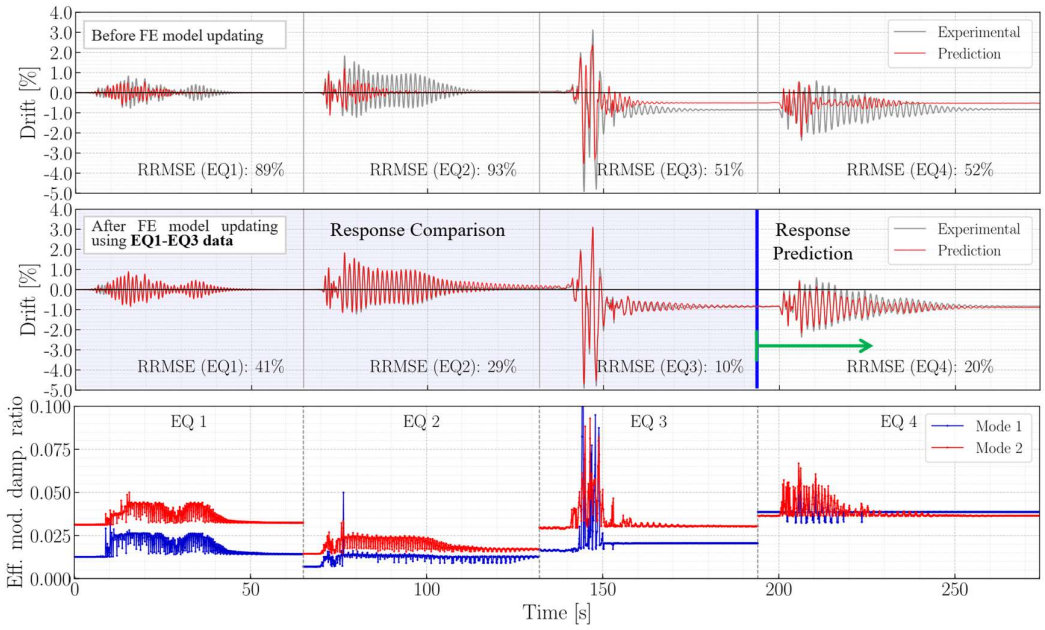


**Figure 5:** Drift response comparison before and after calibration, and evolution of modal damping

The instantaneous generalized modal damping matrices remain predominantly diagonal across all excitations, though off-diagonal terms (of one to two orders of magnitude smaller than the diagonal entries) increase slightly with intensity—indicating weak but growing mode coupling as nonlinear effects develop.

These findings support that the fixed-form Rayleigh model captures amplitude-dependent dissipation indirectly via excitation-specific coefficients. The approach reproduces physically meaningful damping behavior across quasi-elastic to moderately nonlinear regimes, highlighting the robustness and adaptability of the Bayesian updating framework.

## 6 CONCLUSIONS

This study develops and applies a Bayesian FE model updating framework to calibrate nonlinear FE models of RC structures with application to a full-scale RC bridge column tested on the LHPOST at UC San Diego. Using input-output data from three earthquakes (EQ1–EQ3), the model captures the transition from linear to moderately nonlinear flexural response. Calibration targets normalized material, geometric, damping, and noise parameters. TMCMC enables robust posterior sampling under model nonlinearity and high-dimensional uncertainty.

Posterior distributions exhibit strong identifiability for most parameters, with narrow marginal distributions and low coefficients of variation, reflecting the informativeness of the experimental data and the suitability of the selected model structure. Damping parameter pair plots reveal excitation-specific trade-offs consistent with Rayleigh damping. These trends diminish with increasing nonlinearity, as hysteretic dissipation becomes dominant.

Validation shows that the updated model significantly improves response predictions over the prior, with reduced RRMSE across channels. Postprocessed effective modal damping ratios extracted from the calibrated FE model exhibit strong response amplitude dependence both within and across seismic excitations. Their evolution closely follows drift envelopes,

underscoring that effective damping varies with the severity of structural deformation.

Nevertheless, the unexpectedly elevated instantaneous effective modal damping ratios observed under EQ1 highlight persistent challenges. These likely stem from model-form limitations in representing physical damping mechanisms active during low-amplitude, quasi-linear elastic response regimes. Addressing these aspects is a critical next step toward advancing the accuracy and robustness of digital twin frameworks for nonlinear structural systems.

## 7 ACKNOWLEDGEMENTS

Funding for this work by the U.S. Army Corps of Engineers through the U.S. Army Engineer Research and Development Center Research Cooperative Agreement W9132T-22-20014 is gratefully acknowledged.

## REFERENCES

[1] Farrar, C. R. and Worden, K. *Structural Health Monitoring*. Wiley, (2012).
[2] McKenna, F. OpenSees: A Framework for Earthquake Engineering Simulation. *Computing in Science & Engineering*, 13(4), 58–66, (2011).
[3] Ramancha, M. K., Astroza, R., Madarshahian, R., and Conte, J. P. Bayesian updating and identifiability assessment of nonlinear finite element models. *Mechanical Systems and Signal Processing*, 167, 108517, (2022).
[4] Chopra A.K. *Dynamics of Structures: Theory and Applications to Earthquake Engineering*., 6th Edition, Pearson, (2022).
[5] Charney, F. A. Unintended Consequences of Modeling Damping in Structures. *Journal of Structural Engineering*, 134(4), 581–592, (2008).
[6] Petrini, L., Maggi, C., Priestley, M. J. N., and Calvi, G. M. Experimental Verification of Viscous Damping Modeling for Inelastic Time History Analyzes. *Journal of Earthquake Engineering*, 12(sup1), 125–145, (2008).
[7] Simpson, B. and Scott. M. H. Influence of viscous damping models using a constant damping matrix on nonlinear dynamic response. *World Conference on Earthquake Engineering*, WCEE2024, Milan, Italy, (2024).
[8] Sun, L., Conte, J. P., Todd, M. D., Astroza, R., Bock, Y., Offield, G., and Vernon, F. Linear system identification of the UC San Diego Geisel Library building under ambient vibration. *Journal of Civil Structural Health Monitoring*, 15(2), 483–519, (2025).
[9] Ching, J., and Chen, Y.-C. Transitional Markov Chain Monte Carlo Method for Bayesian Model Updating, Model Class Selection, and Model Averaging. *Journal of Engineering Mechanics*, *133*(7), 816–832, (2007).
[10] Schoettler D. C., Restrepo J. I., and Guerrini G. A *Full-Scale, Single-Column Bridge Bent Tested by Shake-Table Excitation*, PEER Report, Vol. 11, No. 3, pp. 555–565, (2015).
[11] Spacone E., Filippou F.C. and Taucer F.F. Fibre beam-column model for non-linear analysis of R/C frames: part I. Formulation, *Earthq Eng Struct Dyn* 25, 711–725, (1996).
[12] Priestley, M. J. N., Calvi, G. M., and Kowalsky, M. J. *Displacement-based seismic design of structures*. IUSS Press, (2007).
[13] Popovics, S. A numerical approach to the complete stress-strain curve of concrete. *Cement and Concrete Research*, *3*(5), 583–599, (1973).
[14] Carreno Vallejos, R. *Characterization of Large Diameter Reinforcement Under Large Strain Cyclic Reversals*. University of California, San Diego, (2018).
[15] Chopra, A. K., and McKenna, F. Modeling viscous damping in nonlinear response history analysis of buildings for earthquake excitation. *Earthq Eng Struct Dyn*, *45*(2), 193–211, (2016).